Scattering of an alkali-metal atomic beam on anti-spin-relaxation coatings

Naota Sekiguchi and Atsushi Hatakeyama*
Department of Applied Physics, Tokyo University of Agriculture and Technology, Koganei, Tokyo 184-8588, Japan

Kazane Okuma and Hiroaki Usui
Department of Organic and Polymer Materials Chemistry, Tokyo University of Agriculture and Technology, Koganei, Tokyo 184-8588, Japan

(Received 6 July 2018; published 29 October 2018)

We performed scattering experiments using a rubidium (Rb) atomic beam on paraffin films and measured the angular and velocity distributions of scattered atoms. The paraffin films were prepared in various ways and characterized by atomic force microscopy and x-ray diffraction. The films exhibited various roughnesses and crystal structures. The paraffin films preserved the spin polarization of the scattered atoms. The measured angular distributions of all prepared films were consistent with Knudsen's cosine law. The velocity distributions were well fitted by Maxwell's distribution, characterized by a temperature much closer to the film temperature than to the atomic-beam temperature. We therefore concluded that the translational motion of the scattered atoms was thermalized with the paraffin films via single-scattering events.

DOI: 10.1103/PhysRevA.98.042709

I. INTRODUCTION

Anti-spin-relaxation coatings on the inner walls of alkali-metal vapor cells are used to preserve the spin polarization of alkali-metal atoms in the cell [1]. Anti-spin-relaxation-coated vapor cells have been applied to experiments requiring a long spin-relaxation time, such as frequency standards [2,3], ultrasensitive magnetometry [4–6], and quantum memory [7]. Recently, novel experimental systems using a coated cell have been reported, e.g., an anti-PT symmetry optical experiment [8] and interferometry using a warm alkali-metal vapor [9]. The behavior of atoms in a coated cell has attracted much attention from the research community.

In the first decade after the discovery of paraffin as an anti-spin-relaxation coating material [1], Bouchiat *et al.* investigated the behavior of alkali-metal atoms on the surface of paraffin [10] and proposed a mechanism to describe their interaction. Alkali-metal atoms adsorb to the coating and remain there for some time before undergoing desorption. The adsorption energy and dwell time on paraffin are 0.1 eV and on the order of a nanosecond, respectively. Adsorption energy and dwell time are important parameters used to characterize the strength of the interactions between atoms and the coating; thus there have been numerous related studies of alkali-metal atoms on paraffin [11–17] and other coating materials, such as octadecyltrichlorosilane (OTS) [15,17–19] and polydimethylsiloxane (PDMS) [20]. Some studies have shown that alkali-metal atoms diffuse into the coating [13,20–22].

The angular and velocity distributions of the desorbed atoms from the coating material also influence the behavior of atoms on the coating [23]. From a practical perspective, the angular and velocity distributions provide insight into the transport of atoms inside a confined device that has a coating [24], given that the effect of atom-surface scattering on the atomic flow becomes more pronounced as the device becomes miniaturized. Additionally, a better understanding of atom transport from the coating will be useful for laser cooling and trapping of short-lived radioactive alkali-metal isotopes [25–28] for electric dipole moment and parity-nonconservation interaction investigations. However, the distributions have been inferred in only a few experiments [29–31]. Some of the experimental results are in good agreement with theoretical predictions in which the angular distribution of the atoms obeys Knudsen's cosine law, a consequence of Maxwell-Boltzmann statistics [30,31]. On the other hand, non-Maxwellian distributions are required to explain the results of other experiments [29]. Notably, the collisions of alkali-metal atoms with background gas should be taken into account in coated cells, given that the mean free path of an alkali-metal atom in background gas as a result of chemical reactions with the coating has been estimated to be shorter than typical cell dimensions [32].

One powerful and direct method used to investigate scattering behavior is scattering of an alkali-metal atomic beam on a coating. To date, scattering experiments involving alkali-metal atomic beams on anti-spin-relaxation coatings have not been reported. There have only been a few scattering experiments of alkali-metal atoms on metals or crystals [33–36], most of which showed that angular distribution followed Knudsen's cosine law and velocity distribution was characterized by a Maxwell distribution via the surface temperature [23,33–36]. In contrast, several experiments involving a LiF crystal [35] and a polished-glass surface [36] reported angular and velocity distributions that were non-Maxwellian.

Here, we report direct measurement of the angular and velocity distributions of rubidium (Rb) atoms scattered from paraffin films. The morphologies of the prepared paraffin films were observed by atomic force microscopy (AFM); the roughness (Ra) of the films differed considerably. The crystal

*hatakeya@cc.tuat.ac.jp

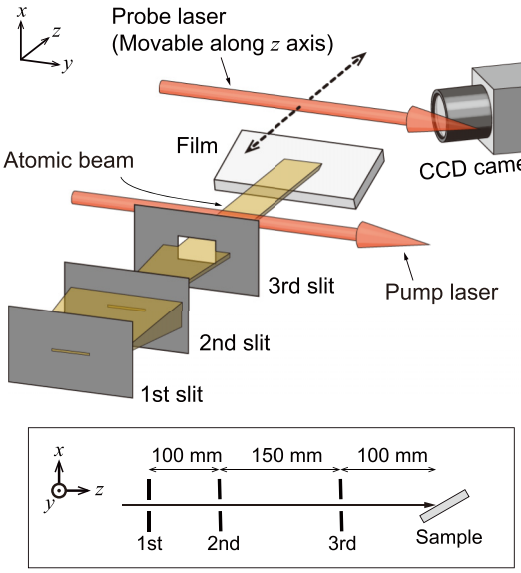

FIG. 1. Schematic diagram of the experiment. The rubidium (Rb) atomic beam was collimated by three slits before colliding with the film. Scattered atoms were detected using probe laser light and a charge-coupled device (CCD) camera. The probe light moved along the z axis. The incident atomic beam was spin polarized by the pump laser light. The inset drawing shows the distances between the slits and the film.

structures were characterized by x-ray diffraction (XRD), which showed that the molecular orientations depended on the film fabrication technique. A Rb atomic beam was scattered by the paraffin films. The anti-spin-relaxation performance of the films was investigated by comparing the spin polarizations of the atomic beam and scattered atoms. The angular and velocity distributions of scattered atoms were examined by detecting laser-induced fluorescence from the atoms. The measured angular distributions of all films were well described by the cosine law. The velocity distributions were well fitted by the Maxwell velocity distribution and were characterized by temperatures much closer to the film temperature than to the atomic-beam temperature. From these results, we concluded that the translational motion of the scattered atoms was well thermalized with the paraffin film surface by single collisions and the spin polarization was preserved.

II. APPARATUS

Figure 1 shows a conceptional sketch of our experiment. The Rb atomic beam emerged from an oven and was collimated using three slits (first, second, and third slits in Fig. 1). The collimated atomic beam collided with the film mounted on a rotational and translational stage. Atoms scattering from the film were illuminated with the probe laser light (diameter: 1.0 mm). The fluorescence induced by the probe light was collected by a charge-coupled device (CCD) camera that was in the y-z plane but not perpendicular to the z axis. The probe light position moved in the z direction during exposure of the CCD camera to the fluorescence. For spin-polarization measurements, the pump light (diameter: 1.5 mm) was introduced upstream of the film. The incident atomic beam was spin polarized using the pump light and the light polarization

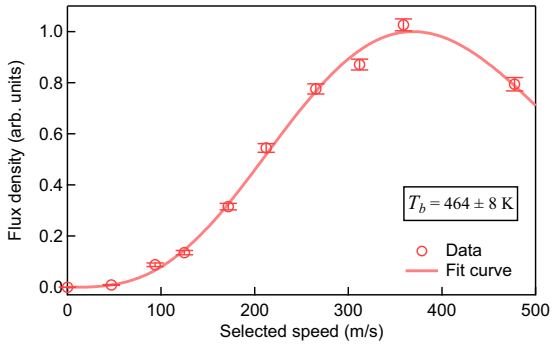

FIG. 2. Flux density $q_b(v)$ of the atomic beam as a function of the speed v of atoms. Data (open circle) were fitted by the fit curve (solid line) given by Eq. (2). The temperature of the atomic beam was estimated to be 464 ± 8 K.

was linear. A beam shutter (not shown in Fig. 1), mounted on a translational stage, was used to block the Rb atomic beam, enabling evaluation of the background signal.

The oven, slits, and film resided in a vacuum chamber maintained at a pressure of a few 10^{-5} Pa. The oven temperature was maintained at 200 °C during measurements and the film was held at room temperature. The three slits were rectangular: the first and second were 0.1×3 mm^2 and the third was 2×3 mm^2. The separations between the first and second, second and third slits, and the third slit and the film were 100 mm, 150 mm, and 100 mm, respectively, as shown in the inset of Fig. 1. As a consequence of the collimation, the angular spread of the Rb atomic beam was 1 mrad along the x axis and 12 mrad along the y axis. The flux of atoms colliding with the film was estimated to be 8×10^{10} s^{-1} based on the oven temperature and slit geometries.

The temperature of the ^{85}Rb atoms in the atomic beam was measured spectroscopically. For temperature measurements, the film was moved out of the path of the atomic beam, and a second laser beam, counterpropagative to the atomic beam, was introduced to the vacuum chamber. The frequency of the laser beam was red-detuned from the resonance frequency of a ^{85}Rb atom at rest. Laser-induced fluorescence from the atoms with a speed v corresponding to the detuning was observed due to the Doppler effect. The intensity of the fluorescence, I_b, was proportional to the number density $n_b(v)$ of atoms having speed v in the atomic beam. Also, the flux density $q_b(v)$ of the atoms with speed v was proportional to the product of the fluorescence intensity and speed v, because the flux density $q_b(v)$ was obtained by multiplying the number density $n_b(v)$ by the atomic speed v,

$$q_b(v) = v n_b(v) \propto v I_b. \tag{1}$$

Figure 2 shows the flux $q_b(v)$ (open circle) as a function of the speed v of atoms. The vertical axis is normalized to show a unit value at the peak. The uncertainty of measurements was estimated based on multiple measurements at a certain velocity; the estimated standard deviations are represented by error bars. The speed distribution $f_b(v)$ of an atomic beam flux is given by

$$f_b(v) = \frac{m^2}{2k_B^2 T_b^2} v^3 \exp\left(-\frac{mv^2}{2k_B T_b}\right), \tag{2}$$

TABLE I. List of films. Film preparation methods, substrates, arithmetic average of the roughness (Ra) within a field of $5\times5\ \mu m^2$ after scattering experiments, and crystalline characteristics after scattering experiments are shown.

	Method	Film	Substrate	Ra (nm)	Molecular orientation
No. 1		SiO_2	Si		
No. 2	Dip coating	Tetracontane	Si/SiO_2	2.6	Normal
No. 3	Vapor deposition	Tetracontane	Borosilicate glass	0.9	Mainly random with some normal and lateral
No. 4	Vapor deposition	Tetracontane	APS monolayer	0.7	Mainly random with some lateral

where m is the mass of a ^{85}Rb atom, k_B is Boltzmann's constant, and T_b is the temperature of the atomic beam. By fitting $f_b(v)$ with a scaling factor to the data $q_b(v)$, as shown by the solid curve in Fig. 2, the temperature T_b was determined to be $T_b = 464 \pm 8$ K, which is consistent with the oven temperature.

III. FILM PREPARATION AND CHARACTERIZATION

The films examined in this study are summarized in Table I. Film no. 1 was a bare Si/SiO_2 plate for comparison, and the other films were tetracontane ($C_{40}H_{82}$, Sigma-Aldrich, >95.0% purity) coated onto substrates.

Tetracontane film no. 2 was prepared on a Si/SiO_2 plate using a dip coating method. Dip coating is commonly used to produce flat, homogeneous films on substrates. A very smooth thin film of tetracontane on a silica substrate can be produced by dip coating [37]. Using an approach similar to that of Ref. [37], we coated the Si/SiO_2 substrate with tetracontane. The silica substrate was cleaned with piranha solution for 10 min in a mixture of 30% hydrogen peroxide (H_2O_2) and 96% sulfuric acid (H_2SO_4) with a volume ratio of 1:3. The cleaned substrate was rinsed with deionized water several times and dried under a flow of nitrogen gas. During the dip-coating process, the substrate and tetracontane in a glass container were placed in an oven at 120 °C. The substrate was dipped into the melted tetracontane and withdrawn at a constant speed. After withdrawal, the oven was cooled slowly. The thickness of film no. 2 was a few hundred nanometers.

Film no. 3 was a tetracontane thin film coated onto a borosilicate-glass substrate by vapor deposition. The glass substrate was washed with detergent and ultrasonically cleaned with deionized water, acetone, ethanol, and methanol. Then, the substrate was dried under nitrogen gas. Tetracontane was evaporated at 300 °C and deposited onto the substrate kept at 30–45 °C for 45 min in a vacuum chamber. The thickness of film no. 3 was 107 nm.

Film no. 4 was also prepared by vapor deposition of tetracontane but onto a self-assembled monolayer (SAM) of 3-aminopropyltrimethoxysilane (APS) on borosilicate-glass. In addition to the cleaning processes for film no. 3, the borosilicate-glass substrate was treated by ultraviolet and ozone exposure. The substrate was then immersed in toluene with 1 wt. % APS for 1 h. After immersion, the substrate was ultrasonically cleaned with toluene for 5 min and dried under a nitrogen atmosphere at 100 °C for 1 h. APS molecules formed a SAM on the glass substrate using this procedure. Vapor deposition of tetracontane onto the APS-SAM was performed using the same procedure as that used for film no. 3. The thickness of film no. 4 was 230 nm.

The tetracontane films were characterized by AFM and XRD analyses. The surface morphologies of film no. 2 before and after the scattering experiments were analyzed by AFM. Figure 3 shows height images of film no. 2 within a field $5\times5\ \mu m^2$. The horizontal direction corresponds to the y axis in Fig. 1. The color scales show the height with respect to the average height over the viewing area. The images show different viewpoints, revealing various modifications of the surface morphologies. The modified surfaces were attributed to the incident atomic beam during the scattering experiments. The arithmetic average of the Ra was evaluated from the heights in the images. The Ra value of film no. 2 decreased

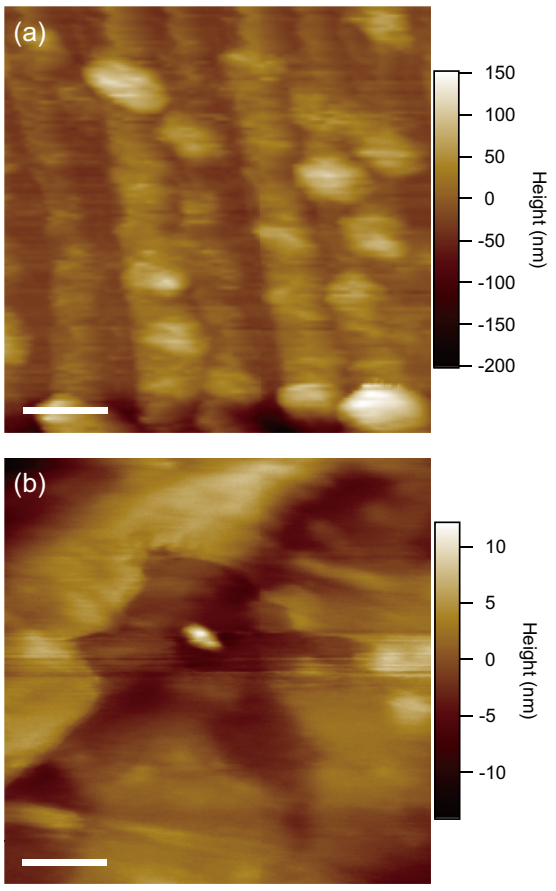

FIG. 3. Atomic force microscopy (AFM) height images of film no. 2 (a) before scattering experiments (Ra = 24 nm) and (b) after scattering experiments (Ra = 2.6 nm). Note the different height scales and AFM viewpoints. The image size was $5\times5\ \mu m^2$, and the white bars indicate 1 μm. Heights of 0 nm represent the average height of the images.

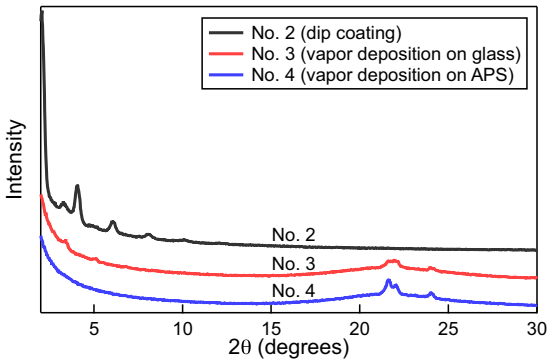

FIG. 4. X-ray-diffraction (XRD) spectra of tetracontane films. The spectra are offset for easier viewing.

from 24 nm (before the scattering experiments) to 2.6 nm (after the scattering experiments). The surface morphologies of films no. 3 and no. 4 after the scattering experiments had Ra values of 0.9 nm and 0.7 nm for films no. 3 and no. 4, respectively.

Figure 4 shows XRD spectra of tetracontane films after the scattering experiments. The horizontal axis represents the diffraction angle 2θ, defined as the angle between incident and diffracted x rays. The vertical axis shows the intensity of the diffracted x rays; spectra are offset vertically for easier viewing. The diffraction peaks at a low diffraction angle, $2\theta \leqslant 10^\circ$, indicate normal molecular orientations [38], and the peaks in the range 20° to 25° indicate lateral molecular orientations [38]. The broad pedestal centered around 21° was attributed to the structure of the borosilicate-glass substrates. Our results show that the tetracontane thin film obtained by dip coating (no. 2) was assembled mainly with normal molecular orientations. In contrast, the films grown by vapor deposition (no. 3 and no. 4) were composed mainly of randomly oriented molecules, because the spectra had small diffraction peaks. Nonetheless, film no. 3 had crystallites with normal and lateral orientations and film no. 4 had crystallites with lateral orientations.

IV. EXPERIMENTS

A. Angular distribution in the x-z plane

We measured the angular distributions of scattered atoms in the x-z plane. The pump light was not used in these measurements. The Rb atomic beam entered the film at an incident angle θ_i defined as the angle from the surface normal. In this study, we fixed $\theta_i \simeq 70^\circ$. Scattered atoms were irradiated by the probe light, which was resonant with the transition $F = 3 \rightarrow F' = 4$ in the D_2 lines of ^{85}Rb (see Fig. 5). The absorption of the resonant probe light led to fluorescence emission from the scattered atoms. Due to velocity selection along the y axis (the laser direction) of around 0 m/s by the Doppler effect, we examined the atoms in the x-z plane. The CCD camera was exposed to the fluorescence for a certain period, while the position of the probe light was scanned along the z axis. The fluorescence images from different positions along z were acquired.

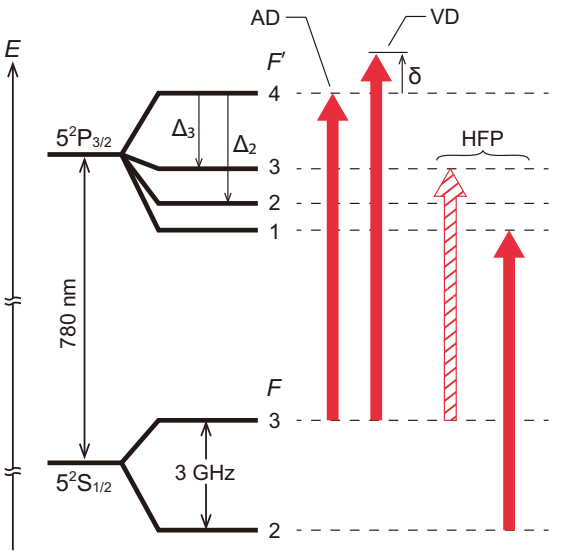

FIG. 5. Energy-level diagram of ^{85}Rb (energy separations not to scale). Energy differences for $F' = 3$ and 2 from $F' = 4$ are denoted by Δ_3 (=121 MHz) and Δ_2 (=184 MHz), respectively. The arrows show the frequencies of the probe laser (filled arrows) and the pump laser (hatched arrow) used in each measurement, angular distribution (AD) measurement, velocity distribution (VD) measurement, and hyperfine polarization (HFP) measurement. The detuning δ of the probe laser for VD measurement can be up to 500 MHz.

Figure 6 shows an example of a fluorescence image. For the image in Fig. 6, fluorescence from scattered atoms was induced by the probe light of 200 μW and recorded with the CCD camera for 228 s. The width w of the atomic beam

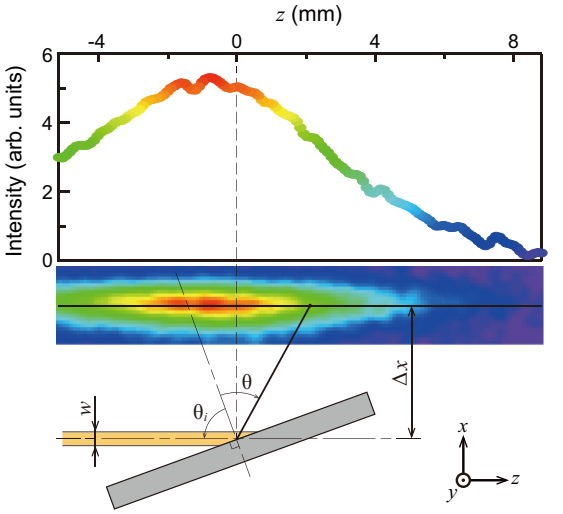

FIG. 6. Fluorescence image in the angular distribution measurement. The geometry of the scattering experiments is illustrated to scale. The solid line in the image indicates the center line of the fluorescence image. The distance of the center line from the atomic beam is denoted by Δx. The upper graph shows the fluorescence intensity $I(z)$ on the center line. When this image was taken, the CCD camera was exposed for 228 s and the probe light power was 200 μW. The other parameters were as follows: $\theta_i = 70^\circ$; $w = 0.5$ mm; $\Delta x = 3.9$ mm.

along the x axis was about 0.5 mm. The distance Δx from the scattering point to the center line of the fluorescence was 3.9 mm. Fluorescence from the background atoms and stray light were eliminated by subtracting the background image taken with the atomic-beam shutter. The solid curve in the upper graph shows the dependence of the fluorescence intensity $I(z)$ on the position of z along the center line of the image. The fluorescence intensity value is indicated by the vertical axis and the curve's color, the color scale of which is the same as that of the fluorescence image. The flux density q of scattered atoms within the scattering angle θ is dependent on the position (r, θ), in polar coordinates, that is, $q = q(r, \theta)$. Here, the scattering angle θ and the distance r from the scattering point are expressed by

$$\theta = \tan^{-1}\left(\frac{z}{\Delta x}\right) + \left(\frac{\pi}{2} - \theta_i\right) \tag{3}$$

and

$$r = \sqrt{\Delta x^2 + z^2}, \tag{4}$$

respectively. Given the angular distribution $s(\theta)$ of scattered atoms, the flux density $q(r, \theta)$ can be expressed by

$$q(r, \theta) = \frac{s(\theta) d\theta}{r\, d\theta}, \tag{5}$$

where the numerator $s(\theta)d\theta$ represents the flux of atoms scattered within the angular range of θ to $\theta + d\theta$, and the denominator $r\, d\theta$ represents the arc length. Similar to Eq. (1), the fluorescence intensity $I(z)$ is proportional to the flux density $q(r, \theta)$,

$$I(z) \propto \frac{q(r, \theta)}{\bar{v}(\theta)} = \frac{s(\theta)}{\bar{v}(\theta) r}. \tag{6}$$

Here, $\bar{v}(\theta)$ is the mean speed of atoms at angle θ. The fluorescence intensity $I(z)$ therefore indicates the angular distribution $s(\theta)$.

B. Velocity distribution along the *y* axis

In this measurement, the position of the probe light was not scanned but fixed at $\theta \sim 0^\circ$, and the pump light was not used. The power of the probe light was 100 μW. The frequency of the probe light was blue-detuned using an acousto-optic modulator (AOM) by an amount of δ from the transition frequency $F = 3 \rightarrow F' = 4$, as shown in Fig. 5. Due to the Doppler effect, scattered atoms moving at velocity v_y along the y axis were selectively detected by the detuned probe light and the CCD camera. The velocity v_y corresponded to the difference between the frequency of the detuned probe light and the transition to the $F' = 2,\ 3,$ or 4 states:

$$v_y = \lambda_0(\delta - \Delta_{F'}), \tag{7}$$

where λ_0 is the wavelength of the D_2 line and $\Delta_{F'}$ is the splitting of the excited states from the $F' = 4$ state in frequency. The transition to $F' = 4$ has the largest absorption cross section among the transitions from the ground state $F = 3$. Furthermore, the excitations to the $F' = 2$ and 3 states depletes the population in the $F = 3$ state, leading to less absorption of the probe light. We therefore considered only the transition $F = 3 \rightarrow F' = 4$ in this measurement. The measurements were repeated with different detuning frequencies δ. The intensities of the fluorescence as a function of the detuning δ reflect the velocity distribution of the scattered atoms along the y axis.

C. Hyperfine polarization

We examined the anti-spin-relaxation performance of the films for the incident atoms. Pump light of 50 μW illuminated the atomic beam in the upper stream of the film, as shown in Fig. 1. The frequency of the pump light was stabilized to the transition $F = 3 \rightarrow F' = 3$ of the D_2 line, as shown in Fig. 5 by the hatched arrow. The pump light selectively excited atoms that had velocity v_y along the y axis around 0 m/s within the velocity width of ~5 m/s corresponding to the natural linewidth of the transition. The velocity selection width was comparable to the velocity width of the atomic beam along the y axis estimated from the angular spread of 12 mrad and the mean speed of ~500 m/s. Consequently, hyperfine polarization of the atoms was produced in every velocity group in the atomic beam, that is, the populations of the ground states were polarized to the $F = 2$ hyperfine state between the ground states $F = 2$ and 3. The probe light of 15 μW was tuned to the transition $F = 2 \rightarrow F' = 1$ of the D_2 line to probe the population in the $F = 2$ state. The fluorescence I_p was induced by the probe light and recorded by the CCD camera. We defined and evaluated the fluorescence difference,

$$\Delta_S = \frac{I_p - I_0}{I_0}, \tag{8}$$

with I_0 as the fluorescence recorded in the absence of hyperfine pumping. Δ_S indicates the difference in the population in the $F = 2$ state from that in the nonpolarized state (thermal equilibrium), given that the fluorescence intensity is proportional to the population in the $F = 2$ state. The difference Δ_B was also evaluated for the incident atomic beam in the same way. For the nonpolarized state, the population in the $F = 2$ state is given by $g_2/(g_2 + g_3) = 5/12$, where g_2 and g_3 are the number of sublevels in the $F = 2$ and $F = 3$ states, respectively. With some algebra, the ratio $P = \Delta_S/\Delta_B$ was derived to be equal to the ratio of the differences in population between the ground states:

$$P = \frac{\Delta_S}{\Delta_B} = \frac{g_2 N_3^S - g_3 N_2^S}{g_2 N_3^B - g_3 N_2^B}. \tag{9}$$

Here, N_F is the population in the ground state specified by F when the atomic beam was hyperfine polarized and the superscripts S and B represent the values for the atomic beam and scattered atoms, respectively. In this study, we measured the ratio P, the surviving hyperfine polarization, for all prepared films.

V. RESULTS AND DISCUSSIONS

Before the measurements, the films were exposed to the atomic beam until the fluorescence from scattered atoms stabilized. We observed that the Si/SiO_2 (film no. 1) required exposure for several hours before the scattering intensity stabilized, whereas the paraffin films were able to scatter atoms shortly after exposure.

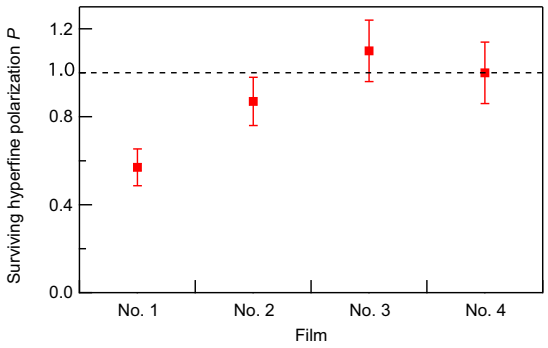

FIG. 7. Surviving hyperfine polarizations of atoms scattered from the films. The vertical axis is normalized by the hyperfine polarization of the incident atomic beam.

The surviving hyperfine polarizations P for films no. 1–4 are shown in Fig. 7. The error bars represent the standard errors of the means. The error was mainly caused by stray light, which was stronger than the fluorescence in the current experimental setup. The dashed line represents the unit value in P and indicates no depolarization by scattering on the films. We confirmed that tetracontane films (no. 2–4) preserved polarization during scattering. It is interesting to note that the uncoated Si/SiO_2 plate (film no. 1) preserved half of the polarization of incident atoms by a single collision.

Figure 8 illustrates the fluorescence intensity $I(z)$ as a function of z, as shown in the upper graph in Fig. 6. The points represent the experimental data and the solid curve is the theoretical curve for an angular distribution that obeys the cosine law, $s(\theta) \propto \cos\theta$ and $\bar{v}(\theta)$ being independent of θ, taking into account the experimental conditions, including the widths of the atomic beam and the shooting angle of the CCD camera. The curve was fitted to experimental data with a scaling factor, which was the only fitting parameter applied. From the figure, the data can be described by the cosine law. The polar plot as a function of the scattering angle θ in the inset of Fig. 8 shows the angular distribution $s(\theta)$. In the derivation of the angular distribution $s(\theta)$ from $I(z)$ using Eq. (6), the mean speed $\bar{v}(\theta)$ was considered independent

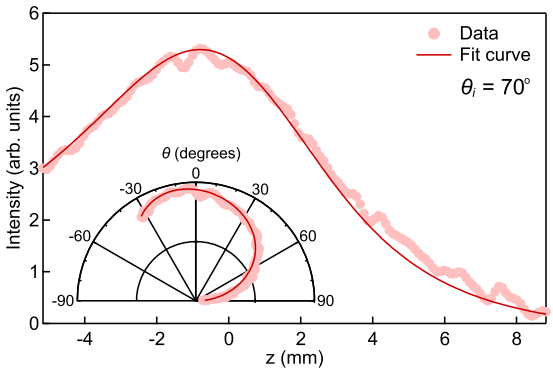

FIG. 8. Fluorescence intensity $I(z)$ as a function of z for film no. 2 at the incident angle θ_i of 70°. The points show the experimental data and the solid curve is the fitted curve based on the cosine law. The inset polar graph shows the angular distribution $s(\theta)$ derived from $I(z)$.

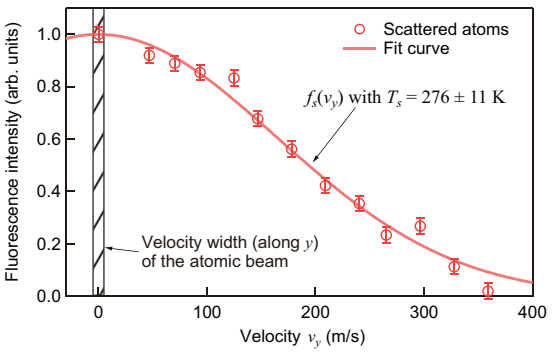

FIG. 9. Distribution of v_y for atoms scattered from film no. 2 (red points). Horizontal axis shows the selected velocity corresponding to the transition $F = 3 \rightarrow F' = 4$. The solid line represents a curve fitted with a Maxwell velocity distribution. The hatched area indicates the velocity width along the y axis of the atomic beam.

from θ, as in the curve fitting. All of the films prepared in this study had angular distributions that were well fitted by the cosine law; however, the films differed with respect to the film material, surface Ra, and molecular orientation. Specular reflection was not found.

The velocity distribution along the y axis is shown in Fig. 9 for film no. 2. The horizontal axis represents the selected velocity v_y described by Eq. (7) with $\Delta_{F'=4} = 0$. The open circles show the fluorescence intensity and the error bars indicate the standard deviation estimated from multiple measurements at a given velocity. The hatched area indicates the typical velocity width along the y axis of the atomic beam. It is clear that the velocities of the scattered atoms were distributed over a much broader range than the velocity distribution of the atomic beam. Curve fitting using Maxwell velocity distribution was considered reasonable, given that the angular distributions followed the cosine law, derived directly from Maxwell-Boltzmann statistics. The Maxwellian fit curve $f_s(v_y)$ shown by the solid line is given by

$$f_s(v_y) = A \exp\left(-\frac{m v_y^2}{2k_B T_s}\right). \tag{10}$$

The amplitude A and the temperature T_s are data-fitting parameters.

As a result of curve fitting, the temperature of the scattered atoms was estimated to be 276 ± 11 K for film no. 2. The temperatures of scattered atoms for all films are shown in Fig. 10. The error bars were obtained from the fitting. If atoms are reflected elastically by a surface that is sufficiently rough for diffusive reflection, the angular distribution corresponds to the cosine law; however, the velocity shows a Maxwellian distribution characterized by the atomic-beam temperature. In fact, the estimated temperatures were clearly lower than the atomic-beam temperature, as shown by the dashed-dotted line in Fig. 10. Moreover, the temperatures were close to the temperature of the film (room temperature), as shown by the dashed line. We therefore concluded, from the cosine-law angular distributions and the temperatures of scattered atoms, that the translational motion of the scattered atoms reached thermal equilibrium with the films.

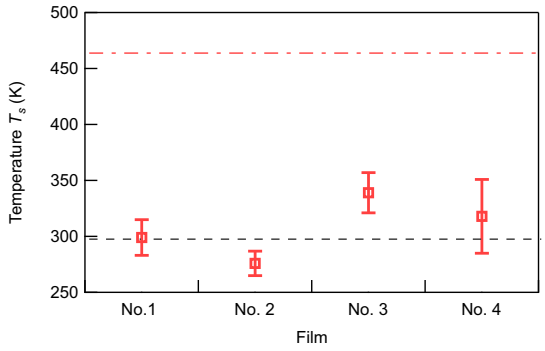

FIG. 10. Temperatures T_s derived from fitting the velocity distribution measurements. The dashed-dotted line (red) and the dashed line (black) show the temperatures of the atomic beam and the films, respectively.

VI. CONCLUSIONS

We performed scattering experiments of an Rb atomic beam on paraffin films. The paraffin films were prepared using several different procedures. The surface morphologies and crystal structures of the prepared films were analyzed by AFM and XRD, respectively. The surface characteristics of the films differed considerably. By comparing the polarizations of the atomic beam and the scattered atoms, we confirmed that the films preserved hyperfine polarization during the scattering process. We then measured the angular and velocity distributions of scattered atoms. Our results indicated that the cosine law well described the angular distributions of all films, despite their different Ra's and crystal structures. The velocity distribution in the direction perpendicular to the incident plane of the atomic beam was fitted by the Maxwell distribution. The temperatures of the scattered atoms for all films were much closer to the film temperature than to that of incident atoms. Based on these results, we conclude that the translational motion of the scattered atoms was well thermalized with the films, and that spin polarization was preserved during the scattering process.

This study has conducted direct measurements of the angular and velocity distributions of alkali-metal atoms scattered by an anti-spin-relaxation coating. Accurate representation of these distributions is essential for efficient loading of alkali-metal atoms in miniaturized coated-device applications, as well as for research that uses short-lived alkali-metal atoms. Further detailed scattering experiments are expected to provide fundamental information on the interactions between alkali-metal atoms and the coating, for example, dwell time measurement via time-of-flight analysis [39].

ACKNOWLEDGMENT

This work was supported by JSPS KAKENHI Grants No. JP15H01013, No. JP17J03089, and No. JP17H02933.

[1] H. G. Robinson, E. S. Ensberg, and H. G. Dehmelt, Bull. Am. Phys. Soc. **3**, 9 (1958).
[2] H. G. Robinson and C. E. Johnson, Appl. Phys. Lett. **40**, 771 (1982).
[3] T. Bandi, C. Affolderbach, and G. Mileti, J. Appl. Phys. **111**, 124906 (2012).
[4] J. Dupont-Roc, S. Haroche, and C. Cohen-Tannoudji, Phys. Lett. A **28**, 638 (1969).
[5] D. Budker, D. F. Kimball, S. M. Rochester, V. V. Yashchuk, and M. Zolotorev, Phys. Rev. A **62**, 043403 (2000).
[6] D. Budker and M. Romalis, Nat. Phys. **3**, 227 (2007).
[7] B. Julsgaard, J. Sherson, J. I. Cirac, J. Fiurasek, and E. S. Polzik, Nature (London) **432**, 482 (2004).
[8] P. Peng, W. Cao, C. Shen, W. Qu, J. Wen, L. Jiang, and Y. Xiao, Nat. Phys. **12**, 1139 (2016).
[9] G. W. Biedermann, H. J. McGuinness, A. V. Rakholia, Y.-Y. Jau, D. R. Wheeler, J. D. Sterk, and G. R. Burns, Phys. Rev. Lett. **118**, 163601 (2017).
[10] M. A. Bouchiat and J. Brossel, Phys. Rev. **147**, 41 (1966).
[11] H. M. Goldenberg, D. Kleppner, and N. F. Ramsey, Phys. Rev. **123**, 530 (1961).
[12] R. G. Brewer, J. Chem. Phys. **38**, 3015 (1963).
[13] V. Liberman and R. J. Knize, Phys. Rev. A **34**, 5115 (1986).
[14] C. Rahman and H. Robinson, IEEE J. Quantum Electron. **23**, 452 (1987).
[15] M. Stephens, R. Rhodes, and C. Wieman, J. Appl. Phys. **76**, 3479 (1994).
[16] D. Budker, L. Hollberg, D. F. Kimball, J. Kitching, S. Pustelny, and V. V. Yashchuk, Phys. Rev. A **71**, 012903 (2005).
[17] E. Ulanski and Z. Wu, Appl. Phys. Lett. **98**, 201115 (2011).
[18] Y. W. Yi, H. G. Robinson, S. Knappe, J. E. Maclennan, C. D. Jones, C. Zhu, N. A. Clark, and J. Kitching, J. Appl. Phys. **104**, 023534 (2008).
[19] K. F. Zhao, M. Schaden, and Z. Wu, Phys. Rev. Lett. **103**, 073201 (2009).
[20] S. N. Atutov, V. Biancalana, P. Bicchi, C. Marinelli, E. Mariotti, M. Meucci, A. Nagel, K. A. Nasyrov, S. Rachini, and L. Moi, Phys. Rev. A **60**, 4693 (1999).
[21] M. Balabas and S. Przhibel'skii, Chem. Phys. Rep. **14**, 882 (1995).
[22] M. V. Balabas and O. Y. Tret'yak, Tech. Phys. **57**, 1257 (2012).
[23] R. E. Stickney, Adv. At. Mol. Phys. **3**, 143 (1968).
[24] M. Giraud-Carrier, T. Decker, J. McClellan, L. Bennett, A. Hawkins, J. Black, S. Almquist, and H. Schmidt, J. Vac. Sci. Technol. A **35**, 031602 (2017).
[25] J. E. Simsarian, A. Ghosh, G. Gwinner, L. A. Orozco, G. D. Sprouse, and P. A. Voytas, Phys. Rev. Lett. **76**, 3522 (1996).
[26] Z.-T. Lu, K. L. Corwin, K. R. Vogel, C. E. Wieman, T. P. Dinneen, J. Maddi, and H. Gould, Phys. Rev. Lett. **79**, 994 (1997).
[27] S. N. Atutov, V. Biancalana, A. Burchianti, R. Calabrese, L. Corradi, A. Dainelli, V. Guidi, B. Mai, C. Marinelli, E. Mariotti, L. Moi, A. Rossi, E. Scansani, G. Stancari, L. Tomassetti, and S. Veronesi, Hyperfine Interact. **146/147**, 83 (2003).
[28] Y. Sakemi, K. Harada, T. Hayamizu, M. Itoh, H. Kawamura, S. Liu, H. S. Nataraj, A. Oikawa, M. Saito, T. Sato, H. P. Yoshida, T. Aoki, A. Hatakeyama, T. Murakami, K. Imai, K. Hatanaka,

T. Wakasa, Y. Shimizu, and M. Uchida, J. Phys.: Conf. Ser. **302**, 012051 (2011).
[29] R. P. Frueholz and J. C. Camparo, Phys. Rev. A **35**, 3768 (1987).
[30] M. Klein, M. Hohensee, D. F. Phillips, and R. L. Walsworth, Phys. Rev. A **83**, 013826 (2011).
[31] X. Zhi-Xiang, Q. Wei-Zhi, G. Ran, H. Xin-Hua, and X. Yan-Hong, Chin. Phys. B **22**, 033202 (2013).
[32] N. Sekiguchi and A. Hatakeyama, Appl. Phys. B **122**, 81 (2016).
[33] J. B. Taylor, Phys. Rev. **35**, 375 (1930).
[34] A. Ellett and V. W. Cohen, Phys. Rev. **52**, 509 (1937).
[35] J. H. McFee, P. M. Marcus, and I. Estermann, Rev. Sci. Instrum. **31**, 1013 (1960).
[36] A. Anderson, S. Haroche, E. A. Hinds, W. Jhe, D. Meschede, and L. Moi, Phys. Rev. A **34**, 3513 (1986).
[37] A. M. Hibberd, S. L. Bergman, Y. L. Zhong, and S. L. Bernasek, J. Chem. Phys. **137**, 174703 (2012).
[38] K. Tanaka, N. Okui, and T. Sakai, Thin Solid Films **196**, 137 (1991).
[39] J. E. Hurst, C. A. Becker, J. P. Cowin, K. C. Janda, L. Wharton, and D. J. Auerbach, Phys. Rev. Lett. **43**, 1175 (1979).